Journal of Power Sources 195 (2010) 6988–6996

Contents lists available at ScienceDirect

Journal of Power Sources

journal homepage: www.elsevier.com/locate/jpowsour

Degradation mechanism of molten carbonate fuel cell based on long-term performance: Long-term operation by using bench-scale cell and post-test analysis of the cell

H. Morita*, M. Kawase, Y. Mugikura, K. Asano

Energy Engineering Research Laboratory, Central Research Institute of Electric Power Industry, 2-6-1 Nagasaka, Yokosuka 240-0196, Japan

ARTICLE INFO

Article history:
Received 31 January 2010
Received in revised form 21 March 2010
Accepted 28 April 2010
Available online 5 May 2010

Keywords:
Molten carbonate fuel cell (MCFC)
Long-term operation
Degradation mechanism
Post-test analysis

ABSTRACT

In order to introduce molten carbonate fuel cells (MCFCs) in commercial applications, the target lifetime of a MCFC has been set at 40,000 h. We have carried out long-term operation tests on several bench-scale MCFCs, which include a 66,000-h continuous operation, and clarified the question of voltage degradation in relation to operating time. We have also carried out post-test analyses on the long-term operated cell components including the electrodes, the electrolyte matrix and the current collectors. The results of the long-term operation and the post-test analyses are described in this paper. The degradation mechanisms of voltage and components are discussed.

© 2010 Elsevier B.V. All rights reserved.

1. Introduction

Molten carbonate fuel cells (MCFCs) are high temperature fuel cells, which achieve a relatively high electrical efficiency and can operate with a number of fuels, ranging from hydrogen to CO-containing gases. Based on these factors, the high temperature operation of MCFCs appears to be a favorable electrochemical power device, but also poses the cell components with unfavorable durability factors. For example, the loss of carbonate electrolyte due to vaporization and the corrosion of the metal components causing voltage degradation to the cell [1,2] or the nickel short circuit of the two electrodes due to the dissolution of the cathode in the electrolyte matrix which limits the lifetime of the cell [3–5].

Regarding the durability of a MCFC on commercial level, it is required a lifetime of 40,000 h and a voltage decay rate of less than 10% after this period. The voltage degradation of a MCFC is generally agreed to be divided into two phases as shown in Fig. 1. The first phase shows a gradual degradation caused by the increase of ohmic resistance (i.e. internal resistance) and the electrode polarization due to the carbonate electrolyte loss. The second phase shows a rapid degradation, which may be caused by Ni short circuit or the gas cross leakage between the electrodes due to the cumulative electrolyte loss over the long period. The transfer from the first phase to the second phase determines the period of operating a MCFC power unit, including stack and inverter, in stable conditions, and that the lifetime when operating the MCFC unit at a higher efficiency and a higher electricity output is probably shorter than the above mentioned period.

It is highly desirable for developers and researchers of fuel cell technologies to assess the operating condition responsible for accelerating the degradation phenomena in the cell and build a model to estimate the lifetime of a fuel cell based on the results of the accelerated testing. Our laboratory has carried out accelerated testing on MCFCs for Ni short circuits by pressurizing bench-scale cells up to about 0.6 MPa and built a model to estimate the beginning of the Ni short circuit phenomenon. On the other hand, the main impact within the operating conditions responsible for accelerating the carbonate electrolyte loss is the operating temperature. It is difficult to build a lifetime model based on the results of the accelerated testing with the electrolyte loss caused by the higher operating temperature since many factors responsible for the electrolyte loss change simultaneously by increasing the temperature. We have, therefore, carried out long-term operation testing on some bench-scale cells at a constant temperature and performed the post-test analyses on the long-term operated cell components instead of carrying out accelerated testing with the electrolyte loss. The results of long-term operation are helpful to identify the degradation mechanism of the MCFC and provide a preliminary understanding for a model that is capable of defining the durability of a MCFC.

* Corresponding author. Tel.: +81 46 856 2121; fax: +81 46 856 3346.
E-mail address: morita@criepi.denken.or.jp (H. Morita).

0378-7753/$ – see front matter © 2010 Elsevier B.V. All rights reserved.
doi:10.1016/j.jpowsour.2010.04.084

Table 1
Specifications of the bench-scale cells used in long-term operation.

Electrode area	110 cm^2
Gas flow	Co-flow
Anode/current collector	Ni–Al, Cr/Ni_{201}
Cathode/current collector	In situ NiO-$MgCO_3$/SUS316L
Electrolyte matrix	γ-$LiAlO_2$ + $LiAlO_2$ fiber or α-$LiAlO_2$ + Al_2O_3 fiber
Electrolyte	Li_2CO_3/Na_2CO_3 = 60/40%

Table 2
Operating conditions used in long-term operation.

Pressure	0.297 MPa
Temperature	600 or 650 °C
Current density	200 mA cm^{-2}
Fuel composition flow rate	H_2/CO_2 = 80/20% + H_2O = 30%
	H_2 utilization = 60%
Oxidant composition flow rate	Air/CO_2 = 90/10% + H_2O = 10%
	O_2/CO_2 utilization = 11/40%

2. Experimental

2.1. Long-term operation

Many post-test analyses with different sized MCFCs show a dependence of the carbonate electrolyte loss on the cell size. The amount of electrolyte loss per unit area increases as the cell size decreases from a commercial stack cell (~1 m^2) to a bench-scale cell (~100 cm^2) [6]. Hence, for the long-term operation of a bench-scale cell, it is necessary to perform a number of carbonate additions into the electrolyte matrix during the operation. The rate of electrolyte loss in a bench-scale cell is relatively large, and the initial amount of carbonate contained in a bench-scale cell is insufficient to maintain the function of the electrolyte matrix such as gas sealing or high ionic conductivity between the electrodes. Tanimoto et al. performed 16 electrolyte additions during the operation to achieve a 40,000 h continuous operation of the bench-scale cell [7].

In order to operate the bench-scale cell for longer than 10,000 h, we used a cell frame with an installed pipe for supplying the additional carbonate electrolyte during the operation. Long-term operation data was obtained using the bench-scale cells manufactured by Ishikawajima-Harima Heavy Industries Co., Ltd. (IHI), the specifications of which are shown in Table 1. IHI applies two different types of material for the electrolyte matrix. One is the γ-phase $LiAlO_2$, which was the standard matrix of FY 2000, the other is the α-phase $LiAlO_2$, which was the standard of FY 2003. It was reported that the α-$LiAlO_2$ was more stable than the γ-$LiAlO_2$ under MCFC operating conditions [8]. Long-term operations were carried out with several pieces of test equipment designed for running bench-scale cells, which can operate the cell up to a temperature of 720 °C and a pressure of 0.7 MPa. Both anode and cathode gas were controlled by a mass-flow-meter (H_2, CO_2 and air). If necessary, the controlled gas mixtures were humidified in response to the temperature of the bubbling vessel before being fed into the cell. The long-term operating conditions are shown in Table 2. In order to establish the oxidant condition of the carbon dioxide, which has the greatest influence on the Ni short circuit phenomenon, a CO_2 composition of 9% was selected for the inlet in reference to a 300 kW-class MCFC/TCG (turbocharger generator) system applied at Kawagoe in Japan [9]. During the operation, an open circuit situation was created once a week to measure the cell voltage (i.e. open circuit voltage), the outlet gas composition by performing a gas chromatography and the internal resistance at a frequency of 1 kHz with a milliohm meter (Hewlett-Packard 4338A). A test that measures cell voltages under load conditions (i.e. output voltages) in several different gas conditions, such as a variation of utilization or the inlet composition, was also run every 2500 h in order to evaluate the time variation of the performance parameters (a, c_1, c_2 and d) in a model described in Section 3.1.

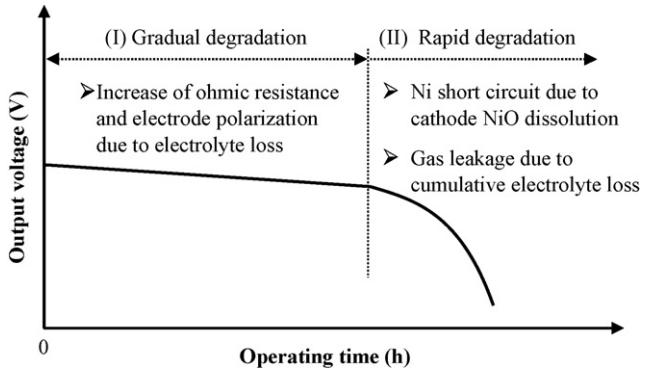

Fig. 1. Schematic diagram of MCFC degradation according to operating time (at a constant current).

2.2. Post-test analyses of cell components after operation

After the long-term operation of the bench-scale cell, the cell was cooled down to room temperature and disassembled into cell components, electrodes, electrolyte matrix and current collectors, in order to execute post-test analyses. If necessary, the disassembled components were immersed in acetic anhydride or a solution of acetic acid for 3 days to dissolve and remove the residual carbonate from the components. Samples of the components were examined with the following equipment: Scanning electron microscope (SEM, Hitachi S-4800), reflected light microscope (Olympus BX60 M), X-ray diffraction spectroscopy (XRD, BrukerAXS D8 ADVANCE VANTEC-1) and inductively coupled plasma atomic emission spectrometer (ICP, PerkinElmer Optima 5300 DV).

3. Voltage degradation model and accelerated testing with Ni short circuit

3.1. Voltage degradation model [10]

The overall reaction of a MCFC is the formation of steam from hydrogen and oxygen, which is provided by the result of the anode reaction according to Eq. (1) and the cathode reaction according to Eq. (2). The field in which the anode reaction of Eq. (1) occurs can be assumed to satisfy the equilibrium of the water gas-shift reaction in Eq. (3).

$$H_2 + CO_3^{2-} \rightarrow H_2O + CO_2 + 2e^-: \quad \text{anode} \tag{1}$$

$$\frac{1}{2}O_2 + CO_2 + 2e^- \rightarrow CO_3^{2-}: \quad \text{cathode} \tag{2}$$

$$CO + H_2O = CO_2 + H_2 \tag{3}$$

Regarding the MCFC performance in practical operating conditions, the following potential balance must be approximately satisfied in the cell.

$$V = E - \eta_{ne} - (R_{ir} + R_a + R_c)J \tag{4}$$

Here V is the output voltage, E the equilibrium potential (i.e. open circuit voltage), η_{ne} Nernst loss, R_{ir} the internal resistance, R_a and R_c the anode and cathode reaction resistance due to the polarization in both electrodes and J the current density. The MCFC degradation phenomenon indicates the first phase as shown in Fig. 1; the decay of the output voltage according to time t is expressed in Eq. (5).

$$V(t) = E - \eta_{ne} - \{R_{ir}(t) + R_a(t) + R_c(t)\}J \tag{5}$$

The variation of the output voltage $V(t)$ can be represented by the increase of R_{ir}, R_a and R_c over time. The increase in the values R_a and

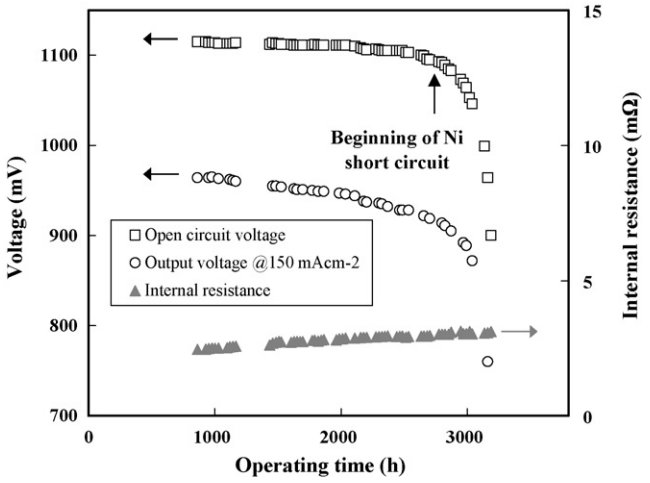

Fig. 2. Accelerated test on showing Ni short circuit. Operating condition is $P = 0.592$ MPa, $T = 650\,^{\circ}C$ and inlet cathode $O_2/CO_2 = 15/85\%$.

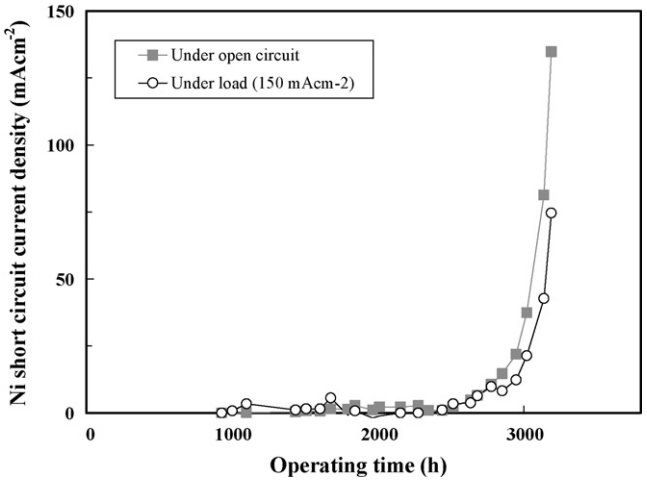

Fig. 3. Current densities due to Ni short circuit under open circuit and load conditions estimated according to the increase of fuel consumption in the accelerated test.

R_c is estimated to be the variation of the performance parameters described in Eqs. (6) and (7).

$$R_a(t) = a(t)P_{H_2}^{-0.5} \tag{6}$$

$$R_c(t) = c_1(t)P_{O_2}^{-0.75}P_{CO_2c}^{0.5} + \frac{c_2(t)}{M_{CO_2c} + d(t)M_{H_2Oc}} \tag{7}$$

Here, P_i or M_i is the reactant partial pressure or composition. a, c_1, c_2 and d are the performance parameters of R_a and R_c, which are determined by using the optimum method to minimize the objective function between the experimental output voltages in several different gas conditions and the calculated output voltages based on Eq. (4). Hence, the term $V(t)$ in Eq. (5), which represents the decay of the output voltage according to time, can be evaluated by measuring and estimating the time variations of R_{ir}, and a, c_1, c_2 and d during operation. The cathode reaction resistance as shown in Eq. (7), including the parameters of c_1, c_2 and d, has been derived from the reactant partial pressure based on the simultaneous diffusion mechanism of the superoxide ion (O_2^-), which corresponds to c_1, and the dissolved CO_2, which corresponds to c_2, in the carbonate melt while taking the effect of water, which corresponds to d, into consideration [11].

3.2. Accelerated testing with Ni short circuit

The Ni short circuit mechanism is based on two reactions. The first is the cathode NiO dissolution in the molten carbonate as expressed in Eq. (8) [12,13]. The second is the Ni deposition in the electrolyte matrix as expressed in Eq. (9). Nickel ions are reduced to metallic nickel in the electrolyte matrix due to the hydrogen diffusing from the anode [4].

$$NiO + CO_2 \rightarrow Ni^{2+} + CO_3^{2-} \tag{8}$$

$$Ni^{2+} + H_2 + CO_3^{2-} \rightarrow Ni + H_2O + CO_2 \tag{9}$$

According to the NiO dissolution reaction in Eq. (8), the high partial pressure of the cathode carbon dioxide accelerates the NiO dissolution phenomenon. For this reason, our laboratory has carried out accelerated tests on Ni short circuits by setting several bench-scale cells at a high partial pressure of cathode carbon dioxide to observe the short circuit phenomenon within a short period of 3000 h. Fig. 2 shows an accelerated test with a Ni short circuit. The values of the open circuit and output voltages fell sharply after 2800 h and the voltage degradation indicated the second phase as shown in Fig. 1. The composition values of hydrogen decreased and those of carbon dioxide increased at the anode outlet after 2800 h. This phenomenon is due to the short circuit between the electrodes, which poses the excessive electrochemical reactions of Eqs. (1) and (2) due to an inner short circuit current. The excessive reactions cause the cell to use more fuel and experience serious voltage degradation. Fig. 3 shows the trends of the excessive current densities due to the Ni short circuit under open circuit and load conditions that have been determined according to the increase of fuel consumption which is based on the variations of hydrogen and carbon dioxide compositions at the anode outlet. Theses trends are similar to the beginning of the Ni short circuit and demonstrate that there is no difference between the estimations made at the beginning, no matter which data is used.

Having summarized the results of the accelerated testing regarding the Ni short circuit, the beginning of the Ni short circuit can be seen as a function of the cathode carbon dioxide partial pressure and the distance between the electrodes (i.e. the thickness of the electrolyte matrix). The equation model for predicting the beginning time t_s is as follows:

$$t_s = K\frac{L^2}{P_{CO_2c,\,in}} \tag{10}$$

Here, K is the coefficient which is dependent on the carbonate composition of the electrolyte or the inhibitory additive to the NiO dissolution etc., L is the electrolyte matrix thickness, $P_{CO_2c,\,in}$ is the partial pressure of the cathode carbon dioxide at the inlet.

4. Results and discussion

4.1. 600 °C–66,000 h operation

A bench-scale cell aiming for long-term operation at 600 °C was installed in the test equipment and began continuous operation in FY 2000. The specification of the electrolyte matrix was γ-phase $LiAlO_2$. This bench-scale cell showed a stable performance while receiving 7 electrolyte additions (2 g per addition). However, the stable performance was interrupted after 66,000 h due to a shutdown of the equipment caused by a human error. For this reason, the bench-scale cell stopped operating at 66,300 h and was then applied in post-test analyses. Figs. 4 and 5 show the results of the long-term operation up to 66,000 h at 600 °C.

Fig. 5 shows the trend of the gas composition at the anode outlet under open circuit and load conditions during the operation. Nitrogen was detected at the anode outlet, which was not contained in the fuel and originated from the cathode air due to the gas cross

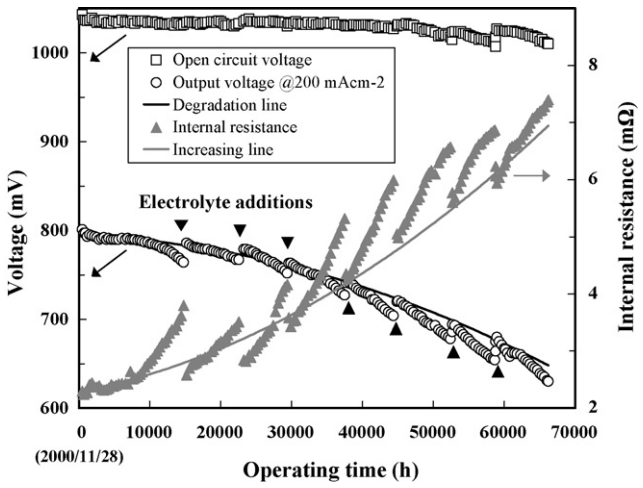

Fig. 4. Long-term operation up to 66,000 h at 600 °C.

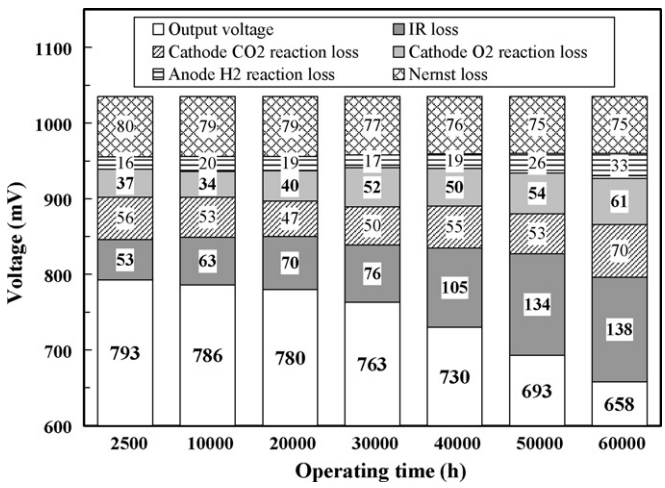

Fig. 6. Analysis of the cell performance at 600 °C according to operating time.

leakage from the cathode to the anode. The values of the nitrogen decreased as soon as an electrolyte addition was made. However, the general trend concerning the nitrogen showed an increase over time. The increase of nitrogen was caused by the declining capability of being able to contain molten carbonate electrolyte in the porous matrix. The reason for the decline appears to be due to the change of $LiAlO_2$ particles composing the electrolyte matrix from the initial fine structure to the coarse one with time. The hydrogen at the anode outlet under both, open circuit and load conditions, decreased over time. However, the values recovered once temporarily after an electrolyte addition was made. The recovered values of hydrogen under open circuit conditions did not recover to the initial level, whereas those of hydrogen under load conditions recovered to a level close to the initial value. The calculation of the fuel consumption based on the hydrogen values, which were subtracted from the hydrogen consumption estimated according to the nitrogen developed due to the gas cross leakage, shows that the fuel consumption remained at the initial value of approx. 60% utilization during operation. The trend of the gas composition at the anode outlet under load conditions, therefore, suggests that the performance of the bench-scale cell up to 66,000 h shows the first phase of degradation as described in Fig. 1.

The trend of the internal resistance R_{ir}, as shown in Fig. 4, shows that the values dropped after each electrolyte addition. These drops contributed towards the improvement of the output voltages. However, the values of internal resistance never restored to the initial level and increased gradually over time, despite several electrolyte additions. Furthermore, the decreasing time of internal resistance became longer after each electrolyte addition; starting from several hours after the 1st addition to several days after the 7th addition. The behavior of the internal resistance described above is due to the decline in the containing capability of the matrix mentioned earlier and/or the increase of the corrosion layer on the metal components such as the current collector.

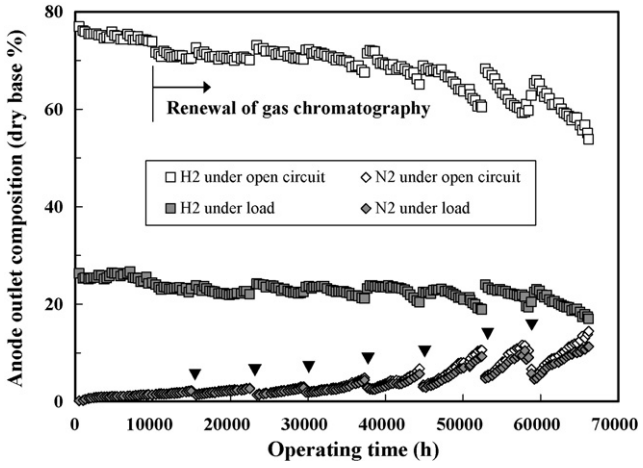

Fig. 5. Gas composition at the anode outlet under open circuit and load conditions during long-term operation at 600 °C.

The trend of the output voltage V, as shown in Fig. 4, shows that the values decrease gradually over time. However, the values increased briefly after each electrolyte addition. If the effect of the electrolyte additions was considered, the degradation of the output voltage would be represented by a solid line as shown in Fig. 4. The degradation line demonstrates that the voltage decay rate is 7% (1.5 mV 1000 h^{-1}) of the initial cell voltage after 40,000 h, 11% (1.7 mV 1000 h^{-1}) after 50,000 and 15% (2.0 mV 1000 h^{-1}) after 60,000 h. The value of 7% meets the target voltage decay rate which is less than 10%. The degradation line is close to the line of a commercial large stack cell (~1 m^2) since the electrolyte loss decreases with the increase of the cell size as mentioned in Section 2.1. Fig. 6 shows an analysis of the cell performance at 600 °C in relation to the operating time. The data is obtained by measuring and estimating the time variations of the performance parameters in the model as described in Section 3.1. The results of Fig. 6 suggest that the main factor responsible for the voltage degradation is the increase of internal resistance R_{ir}. The second factor is the greater cathode oxygen reaction as defined by the c_1 parameter in Eq. (7). As for the time variation in the anode hydrogen reaction as defined by the a parameter in Eq. (6), an increase was observed at 50,000 and 60,000 h. However, the increase of the anode reaction is based on the increase of the gas cross leakage as described in Fig. 5 and becomes almost negligible when considering the hydrogen consumption due to the gas cross leakage after 40,000 h. The reason for the large time variations in the cathode oxygen reaction compared to those of other reactions may be caused by the lower solubility of oxygen in the carbonate melt in comparison to hydrogen or carbon dioxide. The aging cell components, such as electrodes and electrolyte matrix, change the structure of the gas–liquid contact inside the porous electrode where the electrochemical reaction occurs. The change of the structure would be advantageous to increase the cathode oxygen reaction since the amount of reactive oxygen dissolved in the melt is smaller than that of the hydrogen or carbon dioxide.

If we determine a beginning for the Ni short circuit in the 600 °C–66,000 h operation by using Eq. (10), it would be at about 22,000 h. Fig. 7 shows the trend of the excessive current density

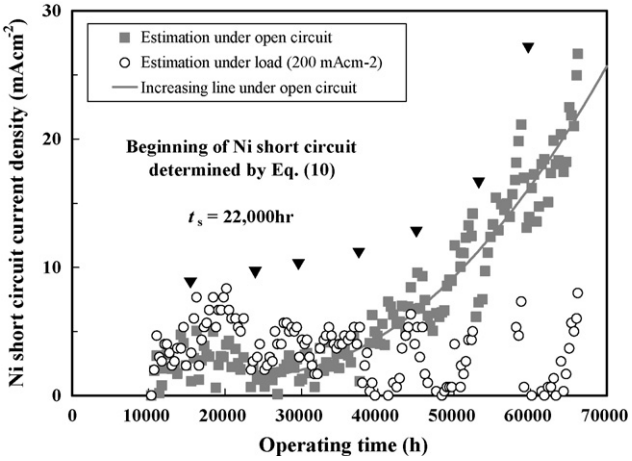

Fig. 7. Current densities due to Ni short circuit based on the increase of fuel consumption estimated according to the anode outlet gas composition in long-term operation at 600 °C.

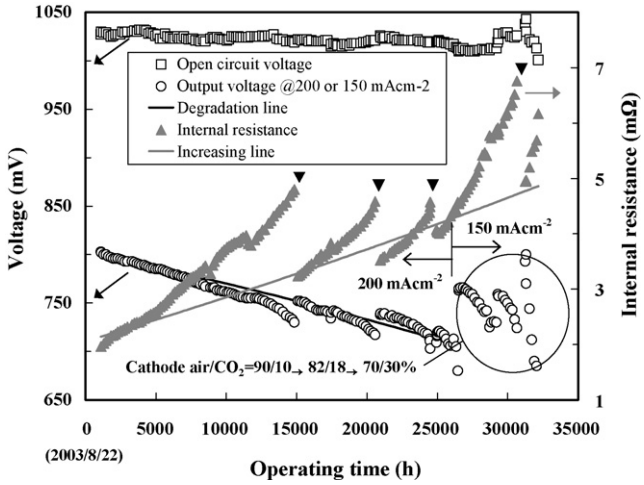

Fig. 8. Long-term operation up to 33,000 h at 650 °C.

due to Ni short circuit estimated according to the increase of fuel consumption under open circuit and load conditions. It can be calculated by using the variations of the gas compositions at the anode outlet as shown in Fig. 5. The current density values due to the Ni short circuit under open circuit conditions begin to increase after 25,000 h. This beginning time is in good agreement with the model designed for accelerated testing. However, the increased current density rate due to the Ni short circuit under open circuit conditions shows values that are one-tenth smaller than the predicted rate based on the accelerated testing. The trend of the Ni short circuit current under load conditions shows that the values of the Ni short circuit current do not indicate a clear short circuit phenomenon. Hence, the results regarding the Ni short circuit in the long-term operation at 600 °C do not always correspond with those of the accelerated testing and imply that the rapid degradation of the Ni short circuit, as described in Fig. 1, may not be caused by the long-term operation of a MCFC's practical atmospheric pressure system.

4.2. 650 °C–33,000 h operation

A bench-scale cell aiming for long-term operation at 650 °C was installed in the test equipment and began its continuous operation in FY 2003. The specification of the electrolyte matrix was α-phase $LiAlO_2$. This bench-scale cell showed a stable performance at a current density of 200 mA cm^{-2} while receiving 3 electrolyte additions (2 g per addition). However, the cell was not able to maintain its stable performance at 200 mA cm^{-2} after 26,500 h since the output voltage of 200 mA cm^{-2} showed a rapid degradation as described in Fig. 1. For this reason, the cell continued operating at a lower current density, 150 mA cm^{-2}, from 26,500 h to 33,000 h and was then applied in the post-test analyses.

Fig. 8 shows the results of the long-term operation up to 33,000 h at 650 °C. The output voltage of 200 mA cm^{-2} decreased over time, however, the values increased briefly after each electrolyte addition. This trend of the output voltage is similar to that of the 600 °C–66,000 h operation. If the effect of the electrolyte additions concerning the output voltage was considered during the operation at 200 mA cm^{-2}, the degradation trend of the output voltage would be represented by a solid line, as shown in Fig. 8. The degradation line demonstrates that the voltage decay rate is 4% (3.3 mV 1000 h^{-1}) of the initial cell voltage after 10,000 h and 8% (3.5 mV 1000 h^{-1}) after 20,000 h. The analysis of the cell performance at 650 °C up until an operating time of 25,000 h shows that the main factor responsible for the voltage degradation is the increase of the internal resistance R_{ir}; the second factor is the increase of the cathode oxygen reaction as defined by the c_1 parameter in Eq. (7). This analysis of the cell performance

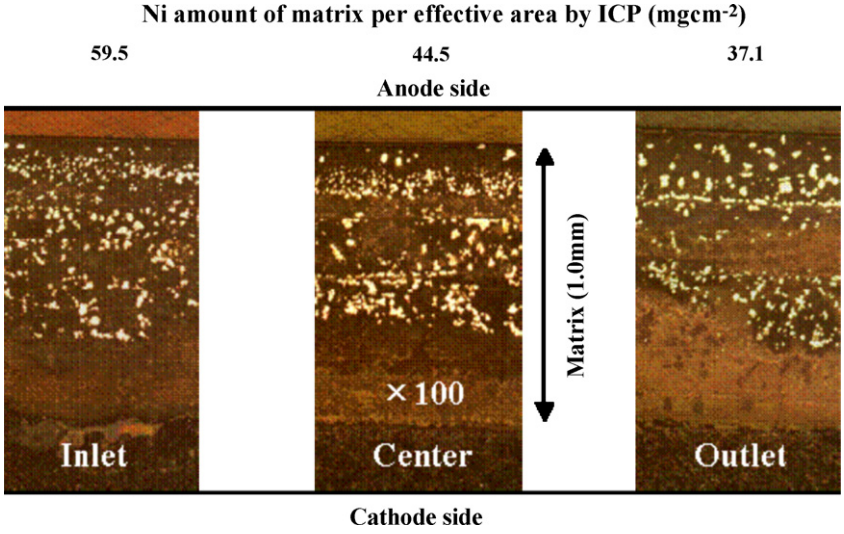

Fig. 9. Cross section images of the electrolyte matrix after 66,000 h operation at 600 °C using reflected light microscope.

is similar to that of the 600 °C–66,000 h operation. The trend of the gas composition during the operation up to 26,500 h points out that the nitrogen values increase and the hydrogen values decrease over time. However, the values recovered temporarily after the electrolyte additions. The alterations concerning the nitrogen and hydrogen gas compositions are similar to those in the 600 °C–66,000 h operation as shown in Fig. 5. Based on the hydrogen values, the fuel consumption was kept at the initial value of approx. 60% utilization during the operation. Hence, the cell performance before 26,500 h never showed any remarkable features due to the Ni short circuit or gas cross leakage.

In order to investigate the reason for the voltage decline after 26,500 h, we changed the gas conditions at the anode and cathode under a current density of 150 mA cm^{-2}. The output voltage at 150 mA cm^{-2} did not show a stable value and decreased gradually within several hours after changing the fuel utilization from 60% to 40% by setting the anode flow rate higher. On the other hand, the output voltage appeared to be sufficiently stable to continue the operation at 150 mA cm^{-2} after changing the cathode gas condition from the initial gas composition (air/CO_2 = 90/10%) to the gas composition close to the stoichiometric ratio (air/CO_2 = 82/18% → 70/30%) by reducing the air flow rate. For this reason, we were able to continue the operation at 150 mA cm^{-2} up to 33,000 h by only changing the gas condition at the cathode, not at the anode. The results above prove that the voltage decline after 26,500 h is not in the anode but in the cathode.

If we determine a beginning for the Ni short circuit in the 650 °C–33,000 h operation by using Eq. (10), the beginning is at about 31,000 h. Judging from the trend of the fuel consumption, which is calculated according to the gas composition values at the anode outlet, the current density due to the Ni short circuit under open circuit conditions begins to increase after 29,000 h. This timing is in good agreement with the prediction. The current density due to the Ni short circuit under load conditions does not indicate a clear short circuit phenomenon. The results of the long-term operation at 650 °C prove that the transfer from the first to the second phase during the operation of a MCFC, as shown in Fig. 1, is not caused by the Ni short circuit but by the cumulative increase of cathode polarization. The cumulative increase of the cathode polarization causes the output voltage to become unstable at 26,500 h.

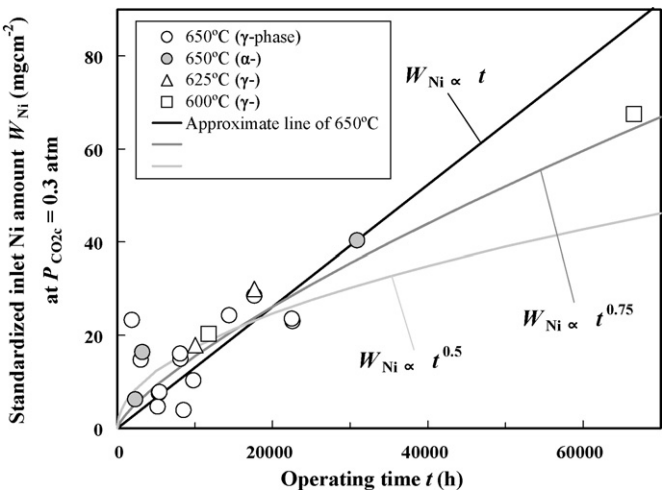

Fig. 10. Dissolved Ni amount of Li/Na carbonate electrolyte matrix after operation.

4.3. Post-test analyses of long-term operated cells

Fig. 9 shows the cross section images of the electrolyte matrix at the inlet, in the center and at the outlet of the bench-scale cell after the 600 °C–66,000 h operation. The gas flow pattern of this cell is co-flow, which means that the location of the anode inlet and outlet is the same as that of the cathode. A lot of white spots are proof of the Ni precipitations caused by the NiO cathode dissolution. The amount of Ni precipitation increases towards the anode as this is where the dissolved nickel ions are reduced to metallic nickels according to Eq. (9). The amount of Ni in the electrolyte matrix at the inlet, in the center and at the outlet is measured to be 59.5, 44.5 and 37.1 mg cm^{-2}, respectively, by using a inductively coupled plasma

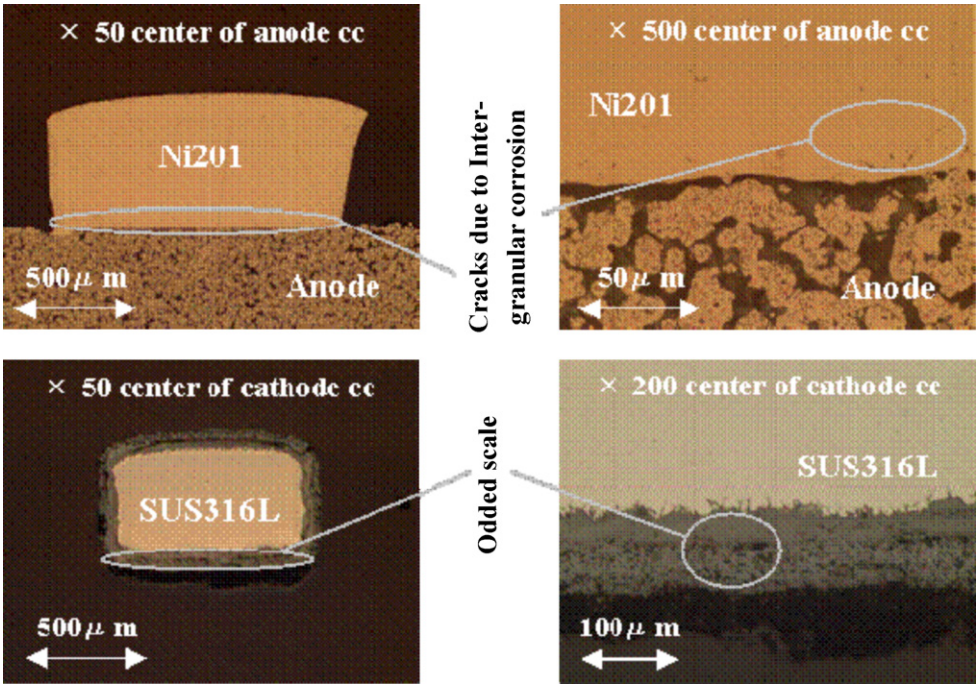

Fig. 11. Cross section images of the anode and cathode current collectors (ccs) after 66,000 h operation at 600 °C using reflected light microscope.

atomic emission spectrometer (ICP). The NiO cathode dissolution mechanism, as expressed in Eq. (8), explains that the Ni increases towards the inlet due to a higher partial pressure of cathode carbon dioxide which accelerates the NiO dissolution. The value of 59.5 mg cm^{-2} at the inlet corresponds with approx. 30% of the initial cathode Ni. The analysis of the dissolved nickel in the electrolyte matrix of the 650 °C–33,000 h operation shows that the Ni distribution was similar to that of the 600 °C–66,000 h cell. The Ni amount in the 650 °C–33,000 h cell at the inlet, in the center and at the outlet is estimated to be 35.6, 28.5 and 27.3 mg cm^{-2} by ICP, respectively. The value of 35.6 mg cm^{-2} at the inlet corresponds with approx. 20% of the initial cathode Ni. Hence, the amount of NiO cathode dissolution is not negligible during long-term operation and is enough to damage the structure of the porous cathode. Fig. 10 shows the summarized data concerning the dissolved nickel in the Li/Na carbonate electrolyte matrix of bench-scale cells manufactured by IHI. The mark corresponding to the Ni amount in the 600 °C–66,000 h cell (□) is close to the approximate 0.75th power line of the 650 °C data ($t^{0.75}$) as shown in Fig. 10. It has been reported that the data relating to the time dependence of the Ni amount ranges from $t^{0.5}$ to t [14], and the temperature dependence of the NiO solubility in the carbonate melt increases with decreasing temperature [13]. Judging from the dependencies of the Ni amount mentioned above, the mark of the 600 °C–66,000 h cell in Fig. 10 is higher than the approximate line of the 650 °C data. The approximate 0.5th power line of the 650 °C data ($t^{0.5}$) meets this requirement.

Fig. 11 shows the cross section images of the anode and cathode current collectors at the center of the bench-scale cell after the 600 °C–66,000 h operation. Cracks due to inter-granular corrosion are visible on the surface of the anode Ni current collector. However, the number of cracks is not worrying and demonstrates that Ni metal has a good durability despite the anode condition of the MCFC. Oxide scale corrosion is observed on the surface of the cathode SUS316L current collector. The maximum thickness of the oxide scale reaches 89 μm on the electrode side and 85 μm on the gas channel side. The sum of scale thickness (174 μm) corresponds to 35% of the initial thickness of the 316L current collector. The cross sections of the current collectors after the 650 °C–33,000 h operation point out that the anode Ni current collector also has a good durability, whereas the cathode 316L current collector shows oxide

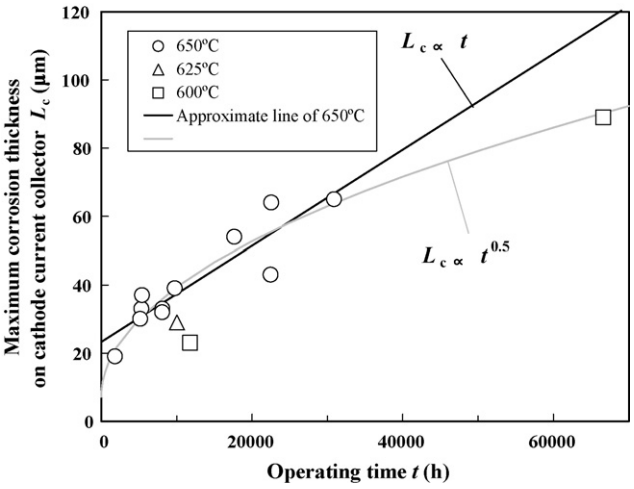

Fig. 12. Maximum corrosion thickness on cathode current collector of Li/Na carbonate cells after operation.

scale corrosion on the surface. The sum of scale thickness (131 μm) after the 650 °C–33,000 h operation corresponds to 26% of the initial thickness of the 316L current collector. These scale thicknesses are responsible for the increase of internal resistance and could cause voltage degradation. Fig. 12 shows the summarized data concerning the maximum corrosion thickness on the cathode current collector of bench-scale cells manufactured by IHI. The mark corresponding to the corrosion thickness of the 600 °C–66,000 h cell is close to the 0.5th power of the 650 °C data ($t^{0.5}$) as shown in Fig. 12. Generally the parabolic rate law ($t^{0.5}$) is applied to the data relating to the time dependence of the corrosion thickness or the ohmic contact resistance between the stainless steel current collector and the cathode up to about 20,000 h [2]. If the parabolic law is applied to the time dependence of the corrosion thickness on the cathode current collector, the mark of the 600 °C–66,000 h cell (□), as shown in Fig. 12, is lower than the approximate line of the 650 °C data since the degree of corrosion in the 600 °C operation is less severe than that of the corrosion in the 650 °C operation. Hence, a linear rate law (t) may be more appropriate for the time

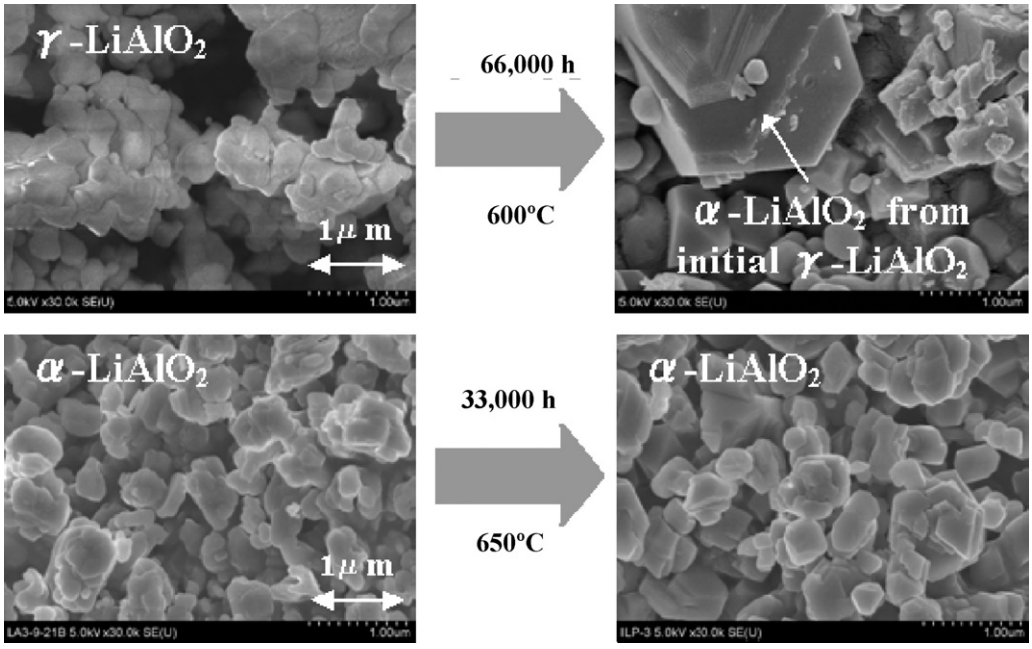

Fig. 13. Electrolyte matrix images before and after the operation using SEM.

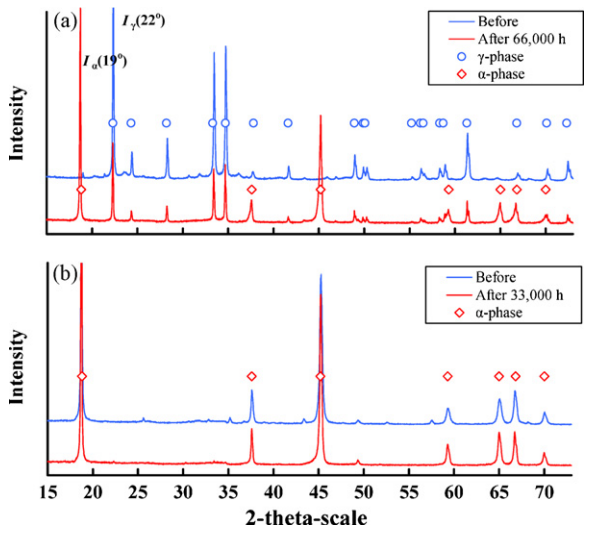

Fig. 14. X-ray diffraction patterns of the $LiAlO_2$ matrix before and after the operation: (a) 600 °C–66,000 h operation; (b) 650 °C–33,000 h operation.

dependence of the maximum corrosion thickness on the cathode current collector.

Fig. 13 shows images of the electrolyte matrix before and after the operation of the 600 °C–66,000 h and the 650 °C–33,000 h cell. The samples from before the operation are the ones kept back and not applied to the operating test. The samples from after the operation are the ones which have had the residual carbonate on the matrix dissolved and removed by using the acetic anhydride or a solution of acetic acid. When comparing the appearance of the $LiAlO_2$ particles before and after the operation on the SEM photo, the α-phase $LiAlO_2$ of the 650 °C–33,000 h cell only shows a slight change in appearance after the operation and a good durability over the long-term operation, whereas the γ-phase $LiAlO_2$ of the 600 °C–66,000 h cell shows severe changes in appearance after the operation with a lot of large and coarse particles. Fig. 14 shows the X-ray diffraction patterns of the $LiAlO_2$ matrix before and after the operation. The XRD patterns of the α-$LiAlO_2$ in Fig. 14(b) show no changes between before and after the operation and maintain their initial pattern even after the 650 °C–33,000 h operation. On the other hand, the XRD patterns of the γ-$LiAlO_2$ before and after the operation in Fig. 14(a) show a phase change from the initial γ to α. In order to estimate the degree of the phase change according to the XRD pattern, as shown in Fig. 14(a), we prepared the samples with different existence ratios between α- and γ-$LiAlO_2$ and measured their XRD patterns. Judging from the peak intensity ratio between $I_\alpha(19°)$ and $I_\gamma(22°)$ in the XRD pattern of Fig. 14(a), approx. 70% of the initial γ-$LiAlO_2$ changed into α-$LiAlO_2$ after the 600 °C–66,000 h operation. The results of the XRD patterns in Fig. 14(a) suggest that the large and coarse particles in Fig. 13 are the transformed particles from the initial γ-$LiAlO_2$ to α-$LiAlO_2$. Hence, the α-$LiAlO_2$ particle is superior to the γ-$LiAlO_2$ particle regarding the durability of the MCFC electrolyte matrix. The stability of the α-$LiAlO_2$ matrix has also been reported by other manufacturers [15].

Regarding the porous structure of the electrode after the operation, there are no severe changes to the anode but instead to the cathode. Fig. 15 shows the cathode images before and after the operation of the 600 °C–66,000 h and the 650 °C–33,000 h cell. The samples from before the operation, which have common specifications for both operations, were kept back and not applied in the operating test. The samples from after the operation are the ones which have had the residual carbonate on the cathode dissolved and removed by using the acetic anhydride or a solution of acetic acid. If the appearance of the NiO particles at the inlet of the cathode is compared before and after the operation in the SEM photo, the NiO particles after the 600 °C–66,000 h operation only show a slight change in appearance even though the amount of dissolved nickel in the matrix reaches about 30% of the initial cathode nickel. The NiO particles after the 650 °C–33,000 h operation show greater changes in appearance since there are now small pin-sized holes on the porous structure of the NiO particles. The number of pin-sized holes increases towards the inlet which corresponds with the trend regarding the dissolved nickel in the electrolyte matrix as shown in Fig. 9. The reason for the difference in the porous structure of the cathode after the operation is not clear. However, the temperature may have an influence on the preferential location of the NiO cathode dissolution. This change to the cathode structure occurring during the 650 °C–33,000 h operation

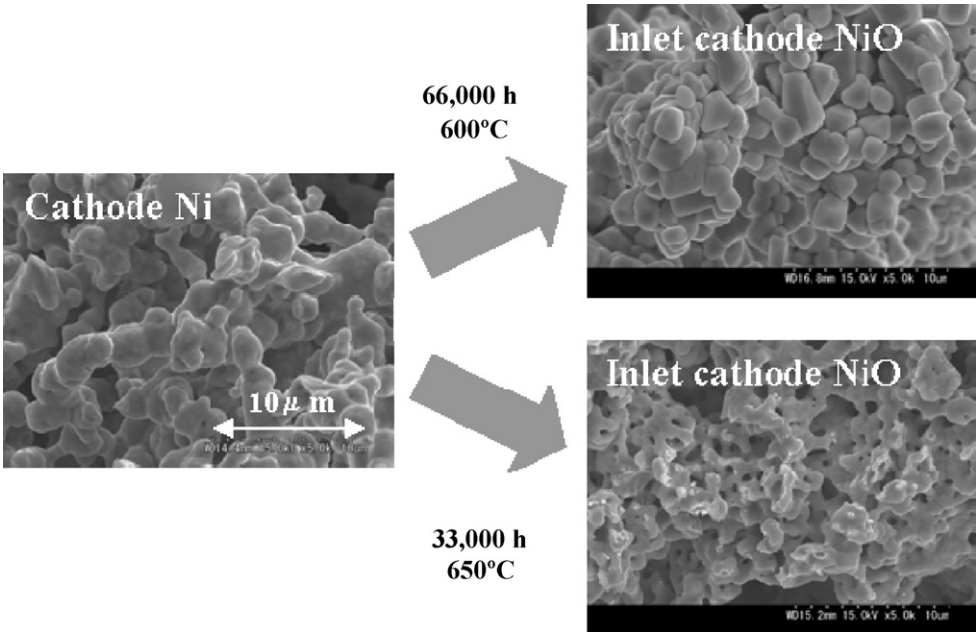

Fig. 15. Cathode images before and after the operation using SEM.

could cause the increase of cathode polarization which makes the output voltage of the bench-scale cell unstable after 26,500 h.

5. Conclusions

According to the results of the 600 °C–66,000 h operation, the performance of the bench-scale MCFC up to 66,000 h indicates the first phase of the MCFC's lifetime which is a gradual degradation as shown in Fig. 1. The voltage degradation model explains that the factor for the voltage degradation during this first phase is mainly caused by an increase of internal resistance, but also due to an increase of the cathode oxygen reaction, whereas an increase of the anode hydrogen reaction is not observed.

According to the results of the 650 °C–33,000 h operation, the performance of the bench-scale MCFC indicates that the transfer from the first to the second phase of Fig. 1 at 26,500 h is not caused by the Ni short circuit but by the cumulative increase of cathode polarization. The post-test analysis implies that the change to the cathode structure caused by the cathode NiO dissolution could be responsible for the second phase, which is a rapid degradation as shown in Fig. 1.

When comparing the results of the 650 °C–33,000 h operation with those of the 600 °C–66,000 h operation, it becomes clear that it is necessary to suppress the operating temperature of the MCFC as much as possible in order to achieve a lifetime over 40,000 h. However, keeping the temperature of the MCFC stack lower during long-term operation not only means a lower performance but also the difficulty of achieving good results. The temperature distribution which indicates the allowance of a higher temperature at the outlet is necessary to cool the stack efficiently under load conditions and control the temperature by a lower gas mass flow when fed into the stack. Hence, we have to select a lower operating temperature in the practical MCFC system while taking the contradictory relation between a high efficiency and a long life into consideration.

Acknowledgements

This work is based on the experimental data collected from a project in the MCFC Research Association from FY 2000 to FY2004. The work was commissioned by NEDO (New Energy and Industrial Technology Development Organization) under the guidance of METI (Ministry of Economy, Trade and Industry). The authors appreciate the advice and support they received. Special thanks to M. Tanno for the long-term operation of the bench-scale cells, and to Y. Masuda, K. Aoki, C. Shoji and K. Yamamasu for the post-test analyses.

References

[1] H. Urushibata, Y. Fujita, T. Nishimura, S. Yoshioka, Denki Kagaku 65 (1997) 121–127 (in Japanese).
[2] S. Frangini, J. Power Sources 182 (2008) 462–468.
[3] Y. Mugikura, T. Abe, S. Yoshioka, H. Urushibata, J. Electrochem. Soc. 142 (1995) 2971–2977.
[4] S. Yoshioka, H. Urushibata, J. Electrochem. Soc. 144 (1997) 815–822.
[5] M. Yoshikawa, Y. Mugikura, T. Watanabe, T. Kahara, T. Mizukami, J. Electrochem. Soc. 148 (2001) A1230–A1238.
[6] Y. Fujita, T. Nishimura, A. Sasaki, T. IEE Jpn. 120-B (2000) 615–620 (in Japanese).
[7] K. Tanimoto, M. Yanagida, T. Kojima, Y. Tamiya, H. Matsumoto, Y. Miyazaki, J. Power Sources 72 (1998) 77–82.
[8] N. Tomimatsu, H. Ohzu, Y. Akasaka, K. Nagagawa, J. Electrochem. Soc. 144 (1997) 4182–4186.
[9] F. Yoshiba, J. Fuel Cell Sci. Technol. 5 (2008) 021010.
[10] H. Morita, M. Komoda, Y. Mugikura, Y. Izaki, T. Watanabe, Y. Masuda, T. Matsuyama, J. Power Sources 112 (2002) 509–518.
[11] T. Nishina, S. Ohuchi, K. Yamada, I. Uchida, J. Electroanal. Chem. 408 (1996) 181–187.
[12] C.E. Baumgartner, J. Electrochem. Soc. 131 (1984) 1850–1851.
[13] K. Ota, S. Mitsushima, S. Kato, S. Asano, H. Yoshitake, N. Kamiya, J. Electrochem. Soc. 139 (1992) 667–671.
[14] Th. Brenscheidt, F. Nitschké, O. Söllner, H. Wendt, Electrochim. Acta 46 (2001) 783–797.
[15] M. Farooque, H.C. Maru, J. Power Sources 160 (2006) 827–834.